Interstellar deuterated ammonia: from NH3 to ND_3

Evelyne Roueff, Darek C. Lis, F. F. S. van der Tak, Maryvonne Gerin, Paul F. Goldsmith

A&A 438, 585–598 (2005)
DOI: 10.1051/0004-6361:20052724

Astronomy & Astrophysics

Interstellar deuterated ammonia: from NH_3 to ND_3

E. Roueff[1], D. C. Lis[2], F. F. S. van der Tak[3], M. Gerin[4], and P. F. Goldsmith[5]

[1] Laboratoire Univers et Théorie, UMR 8102 du CNRS, Observatoire de Paris, Section de Meudon, Place Jules Janssen, 92195 Meudon, France
e-mail: evelyne.roueff@obspm.fr
[2] Downs Laboratory of Physics 320-47, California Institute of Technology, Pasadena, CA 91125, USA
[3] Max-Planck-Institut für Radioastronomie, Auf dem Hügel 69, 53121 Bonn, Germany
[4] Laboratoire d'Étude du Rayonnement et de la Matière en Astrophysique, UMR 8112 du CNRS, Observatoire de Paris and École Normale Supérieure, 24 rue Lhomond, 75231 Paris Cedex 05, France
[5] Department of Astronomy and National Astronomy and Ionosphere Center, Cornell University, Ithaca, NY 14853, USA

Received 18 January 2005 / Accepted 4 April 2005

Abstract. We use spectra and maps of NH_2D, ND_2H, and ND_3, obtained with the CSO, IRAM 30 m and Arecibo telescopes, to study deuteration processes in dense cores. The data include the first detection of the hyperfine structure in ND_2H. The emission of NH_2D and ND_3 does not seem to peak at the positions of the embedded protostars, but instead at offset positions, where outflow interactions may occur. A constant ammonia fractionation ratio in star-forming regions is generally assumed to be consistent with an origin on dust grains. However, in the pre-stellar cores studied here, the fractionation varies significantly when going from NH_3 to ND_3. We present a steady state model of the gas-phase chemistry for these sources, which includes passive depletion onto dust grains and multiply saturated deuterated species up to five deuterium atoms (e.g. CD_5^+). The observed column density ratios of all four ammonia isotopologues are reproduced within a factor of 3 for a gas temperature of 10 K. We also predict that deuterium fractionation remains significant at temperatures up to about 20 K. ND and NHD, which have rotational transitions in the submillimeter domain are predicted to be abundant.

Key words. ISM: molecules – molecular processes – stars: circumstellar matter – stars: formation

1. Introduction

In recent years, the chemistry of dense cores has been revised with the almost simultaneous discovery of multiply deuterated molecules (D_2CO: Turner 1990; Ceccarelli et al. 1998; ND_2H: Roueff et al. 2000; ND_3: Lis et al. 2002b; van der Tak et al. 2002; CHD_2OH, CD_3OH: Parise et al. 2002, 2004) on the one hand, and of very large depletions of CO on the other hand (Bacmann et al. 2002). In fact, the two processes are closely related since the condensation of CO and other abundant gas phase molecules favors deuterium fractionation, by decreasing the destruction rate of deuterated molecular ions (Bacmann et al. 2003). As multiply deuterated molecules are found in dense cores prior to star formation (as in Barnard 1 and LDN 1689N), or in very young protostars (as in NGC 1333 IRAS 4A), they can be used for studying and identifying the earliest stages of star formation. While an analysis of the line profiles gives clues about the gas dynamics in the envelope surrounding the protostar, or in the dense core, the molecular abundance and especially the fractionation provides information on the physical conditions (temperature, depletion) and on the chemistry. It is therefore of interest to improve our understanding of deuterium chemistry. For this purpose, accurate fractionation ratios are needed for multiply deuterated molecules.

Two main paths are invoked for understanding the large deuterium fractionation observed in dense cores. The first is based on gas phase chemistry and invokes the ion-molecule deuterium exchange reactions taking place at low temperatures, as first proposed by Watson (1974). In this framework, deuterated molecules are built in successive reactions starting with either H_2D^+ (and also D_2H^+ and D_3^+), CH_2D^+ or C_2HD^+ (Roberts & Millar 2000; Roberts et al. 2003; Gerlich et al. 2002). The confirmed detections of H_2D^+ in the envelopes of disks encompassing the protostars NGC 1333 IRAS 4A and IRAS 16293-2422 (Stark et al. 1999; Stark et al. 2004) and in the pre-stellar core LDN 1544 (Caselli et al. 2003), as well as the recent detection of D_2H^+ in LDN 1689N (Vastel et al. 2004), have provided strong observational support for this theory. The second path for forming deuterated molecules is based on grain chemistry (Tielens 1983). As hydrogenation on grain mantles has been proposed to explain the large abundances of solid phase CH_3OH (Dartois et al. 1999; Gibb et al. 2000; Pontoppidan et al. 2003), the analogous process with deuterium would build deuterated molecules on grains. Because in dense cores, the gas phase abundance ratio of atomic D/H is probably

orders of magnitude larger than the elemental abundance ratio of 1.5×10^{-5}, the surface chemistry leads also to large deuterium fractionation, which scales as the (gas-phase) D/H ratio[1]. While the surface processes seem interesting, there is no secure confirmation of the role of dust mantles for deuterium fractionation, as neither HDO nor deuterated methanol has yet been detected in the solid phase (Dartois et al. 2003; Parise et al. 2003).

These two paths may lead to different fractionation ratios for multiply deuterated molecules (Rodgers & Charnley 2001), because the formation of deuterated molecules involves largely different processes and chemical reactions. For gas phase processes, the fractionation ratio at each stage results from competing chemical reactions (fractionation reactions substituting deuterium atoms for hydrogen atoms, destruction reactions with other molecules and dissociative recombination reactions removing the fractionation, etc.). The fractionation ratio must be calculated with a comprehensive chemical model and is expected to be different for the different stages of deuterium fractionation of a given species, since the specific reactions are different. In a simple model of grain surface chemistry, the abundance ratios of various deuterated species are expected to be similar, since each such ratio is proportional to the gas phase D/H abundance ratio. For all bonds with a heavy atom, the probability of bonding with a H or D atom scales with the deuterium/hydrogen ratio. All bonds behave independently in this process.

Four different isotopologues of ammonia, including fully deuterated ammonia, ND_3, as well as NH_2D and ND_2H, can be observed in dense cores. The ammonia data can thus provide the information required for understanding the formation of multiply deuterated molecules in dense cores. This paper presents new data on deuterated ammonia in a small sample of dense cores, some of which are forming stars. The observations are presented in Sect. 2, and the results described in Sect. 3. Section 4 presents comprehensive gas phase chemical models aimed at understanding the roles of gas density, depletion, and temperature in the fractionation of ammonia. We summarize our results in Sect. 5.

2. Observations

The rotational transitions and frequencies of the various isotopologues of ammonia that have been observed are shown in Table 1. The frequencies refer to the strongest hyperfine component. For Einstein A-values and statistical weights, see Tiné et al. (2000) (NH_2D), Roueff et al. (2000) (ND_2H) and van der Tak et al. (2002) and Lis et al. (2002b) (ND_3).

2.1. Millimeter-wave observations

Observations of NH_2D and ND_2H lines near 110, and 220 GHz were carried out at the 30-m telescope of the Institut de Radio Astronomie Millimétrique (IRAM) on Pico Veleta, Spain, in August 2002. We also use additional 86 GHz observations performed in November 2001 and September 2002. The front ends were the facility receivers A100, B100, A230 and B230, and the back end was the Versatile Spectral and Polarimetric Array (VESPA) autocorrelator. During night time, the weather was good, with ≈4 mm of precipitable water vapour and $T_{\rm sys} \approx 140$ K at 110 GHz, while during daytime, the water column and $T_{\rm sys}$ roughly doubled. At 110 GHz, the telescope has a *FWHM* beam size of 22″. The pointing of the telescope was stable to within 2 arcsec. Data were calibrated onto a $T_{\rm mb}$ scale by multiplying by 1.25, the ratio of the forward coupling efficiency to the main beam efficiency.

Sources were selected from Shah & Wootten (2001) to have high NH_2D column densities, but the positions used here are from Jijina et al. (1999) for Orion and Monoceros and from McMullin et al. (2000) for Serpens. Table 2 lists source positions and LSR velocities. Only upper limits were obtained toward NGC 2264G and CB 17.

To locate the "deuterium peak" in each source, maps were made of the NH_2D $1_{11} \rightarrow 1_{01}$ emission near 110 GHz. These maps include up to 18 points, at half-beam (11″) spacing. In the case of NGC 1333, a 55-point map was made,

[1] This paper uses full names (e.g., deuterium) to denote elements, and symbols (e.g., D) to denote atomic species.

Table 1. Parameters of observed rotational transitions.

Species	Transition	$E_{\rm u}$	ν
		K	MHz
NH_2D	$1_{11}-1_{01}$	20.7	85 926.3
NH_2D	$1_{11}-1_{01}$	21.3	110 153.6
ND_2H	$1_{10}-1_{01}$	18.7	110 812.9
ND_2H	$1_{10}-1_{01}$	18.4	110 896.7
ND_2H	$2_{20}-2_{11}$	56.8	206 971.9
NH_2D	$3_{22}-3_{12}$	120.	216 562.6
ND_3	$1_{01}-0_{00}$	14.9	309 909.7

Table 2. Positions and velocities of the observed sources.

Source	RA	Dec	$V_{\rm LSR}$
	J2000	J2000	km s^{-1}
NGC 1333	03:29:10.3	+31:13:32.2	7.0
Barnard 1	03:33:20.8	+31:07:34.8	6.8
LDN 1544C	05:04:16.6	+25:10:47.8	7.4
OMC 2	05:35:26.3	–05:09:49.4	11.2
HH 1	05:36:17.3	–06:46:08.2	9.2
LDN 1630	05:46:07.4	–00:13:41.8	10.0
NGC 2264C	06:41:11.6	+09:29:25.1	8.0
LDN 134N	15:54:08.5	–02:52:01.0	2.4
LDN 1689N	16:32:29.5	–24:28:52.6	3.8
LDN 483	18:17:29.7	–04:39:38.3	5.5
S 68N	18:29:47.5	+01:16:51.4	8.5
NGC 2264G	06:41:11.0	+09:56:00.8	4.6
CB 17	04:04:38.0	+56:56:11.0	–4.6

encompassing the locations of both previous ND_3 detections. The integration time was 2 min per point, using frequency switching with a frequency shift of 8 MHz. Subsequently, deep integrations on the ND_2H lines were performed at the locations of the NH_2D peaks.

2.2. Submillimeter-wave observations

Submillimeter observations were carried out in 2002 and 2003 using the 345 GHz facility receiver and spectrometers of the Caltech Submillimeter Observatory (CSO) on Mauna Kea (Hawaii). The data were taken under average weather conditions (225 GHz zenith opacity ∼0.1). The CSO *FWHM* beam size at 309 GHz is ∼25″, and the main beam efficiency at the time of the observations, determined from total-power observations of planets, was ∼60%. Typical calibration uncertainties are ∼25%. The pointing of the telescope was stable to within 5 arcsec. We used the 1.5 GHz, 500 MHz, and 50 MHz bandwidth acousto-optical facility spectrometers. The spectral resolution of the high-resolution, 1024 channel 50 MHz spectrometer is ∼0.15 MHz or 0.15 km s^{-1}. All spectra were taken in the double beam switched observing mode with a secondary chopper throw of 180″.

2.3. Centimeter-wave observations

Observations of the ND_3 inversion lines in the Barnard 1 cloud were carried out between 2003 October 31 and November 11 at the Arecibo Observatory in Puerto Rico, using the new *L*-Band Wide facility receiver. Four subcorrelators of the interim spectrometer system were used, each having 1024 lags. A high-resolution subcorrelator with a total bandwidth of 0.781 MHz (0.144 km s^{-1} velocity resolution) was centered on the frequency of the strongest ND_3 hyperfine component, 1589.0178 MHz (Table 7). Two additional subcorrelators with bandwidths of 3.125 MHz, centered on the frequencies of 1588.4043 and 1588.6316 MHz, covered the remaining ND_3 hyperfine components with a velocity resolution of 0.576 km s^{-1}. In addition, a 1.563 MHz bandwidth subcorrelator, centered on the frequency of the 1667.3590 MHz OH line, was used to monitor system performance during the long integration. Quasars B02231+313 and B0340+048 were used for pointing and calibration. The data were taken in position switching mode with the reference position at a right ascension offset by 5 min of time. The typical system temperature referred to above the earth's atmosphere was ∼25 K. The total on source integration time was 756 min. The main beam plus first sidelobe efficiency of the Arecibo Telescope is ∼70% at 1.6 GHz.

3. Results

3.1. Maps of NH_2D emission

Figures 1 to 6 show the spatial distribution of NH_2D emission as observed with the IRAM 30 m. In Barnard 1 and HH-1, the emission has a distinct peak at a slight offset from our nominal central position given in Table 2. On the other hand, the

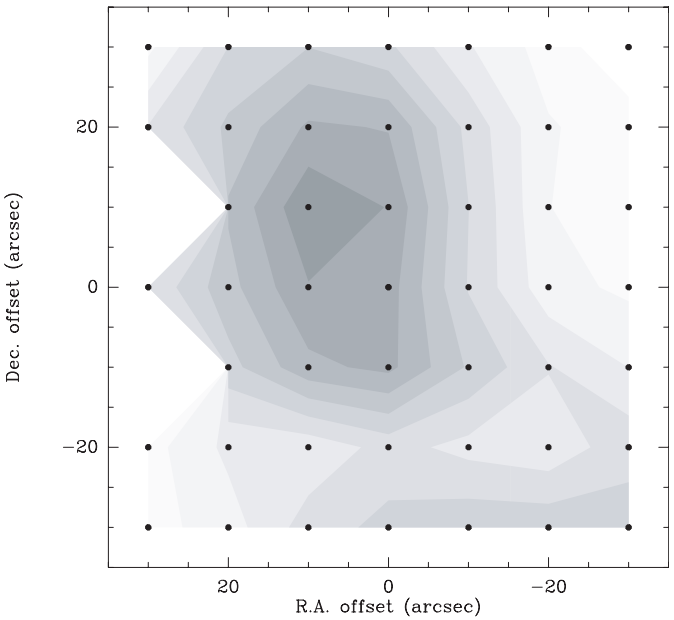

Fig. 1. Map of $\int T_{\rm mb} {\rm d}V$ of the main hyperfine component of the NH_2D $1_{11}-1_{01}$ (ortho) 85.9 GHz transition in Barnard 1. The coordinates of the (0, 0) position are RA(J2000) = 03:33:20.8, Dec(J2000) = +31:07:34.8. Greyscale steps are: 0.5 to 5.0 by 0.5 K km s^{-1}.

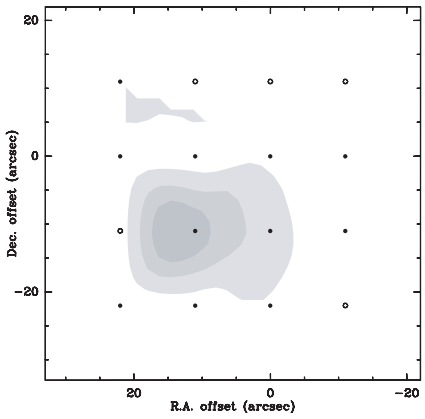

Fig. 2. Map of the integrated NH_2D $1_{11}-1_{01}$ (para) 110.2 GHz emission in HH-1. The coordinates of the (0, 0) position are RA(J2000) = 05:36:17.3, Dec(J2000) = −06:46:08.2. Greyscale steps are 0.3 to 0.6 by 0.15 K km s^{-1}. Unfilled circles denote positions where no emission was detected.

emission in OMC-2, S68N and NGC 2264C is not strongly peaked. The map of NGC 1333 indicates that NH_2D does not peak at the position of the protostar IRAS 4A at (0, 0). Instead, the emission peaks in two lobes, one located 10–20″ N of IRAS 4A and the other to the W-SW of it, roughly between offsets (20, 0) and (30, −20). This distribution follows that of the DCO^+ 3→2 emission, mapped at the CSO by Lis et al. (2004), and is consistent with the observation that the ND_3 emission in NGC 1333 is stronger at the offset position (23, −6) than at IRAS 4A (van der Tak et al. 2002).

Table 3 reports the column density of NH_2D at those positions where the fitting of the hyperfine structure was successful, calculated following Tiné et al. (2000). Emission of NH_2D is clearly detected in other cases, as displayed in the maps,

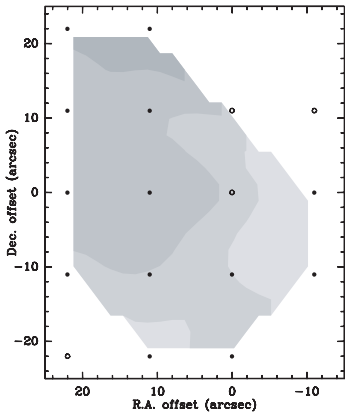

Fig. 3. As previous figure, for OMC-2. The coordinates of the (0, 0) position are RA(J2000) = 05:35:26.3, Dec(J2000) = −05:09:49.4. Greyscale steps are 0.1 to 0.5 by 0.1 K km s^{-1}.

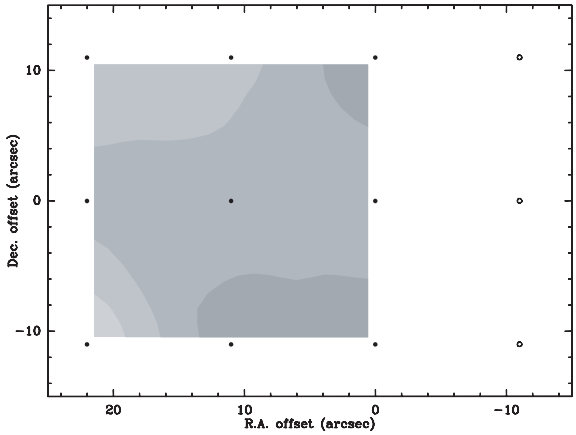

Fig. 4. As previous figure, for S68N. The coordinates of the (0, 0) position are RA(J2000) = 18:29:47.5, Dec(J2000) = +01:16:51.4. Greyscale steps are 0.1 to 0.7 by 0.1 K km s^{-1}.

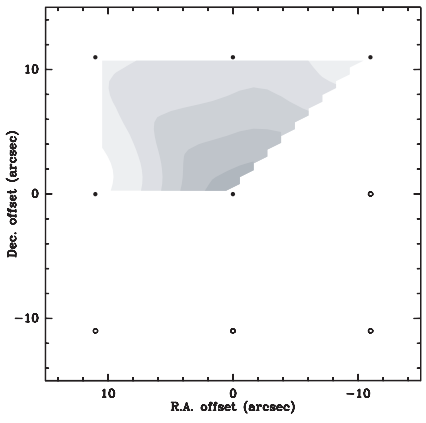

Fig. 5. As previous figure, for NGC 2264C. The coordinates of the (0, 0) position are RA(J2000) = 06:41:11.6, Dec(J2000) = +09:29:25.1. Greyscale steps are 0.1 to 0.7 by 0.1 K km s^{-1}.

but no optical depth could be derived as the individual spectra have a low signal to noise ratio. The HFS method within the CLASS package gives the total optical depth of the line and the radiation temperature, assuming a beam filling factor of unity. Since this latter assumption may not always be

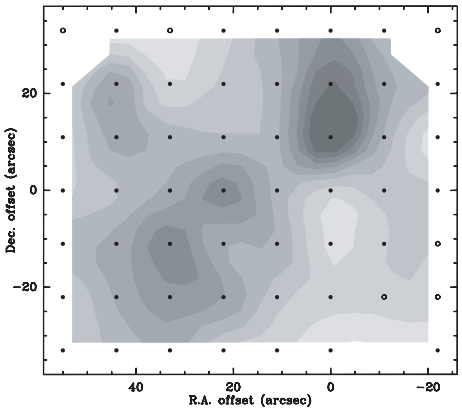

Fig. 6. As previous figure, for NGC 1333. The coordinates of the (0, 0) position are RA(J2000) = 03:29:10.3, Dec(J2000) = +31:13:32.2. Greyscale steps are 0.1 to 0.9 by 0.1 K km s^{-1}.

fulfilled, the table also gives column density estimates for the cases $T_{ex} = 5$ K and 10 K. We calculated the partition functions at these two considered temperatures. The partition functions of NH_2D, ND_2H, and ND_3 for an excitation temperature of 10 K are 9.37, 9.51, and 38.3, respectively. The corresponding values for $T_{ex} = 5$ K are 4.47, 4.21, and 17.23, respectively.

The absence of an NH_2D peak at NGC 1333 IRAS 4A could partly be due to excitation effects. However, the $3_{22} \rightarrow 3_{12}$ line of NH_2D is not detected at this position. The upper limits for this line in NGC 1333, Barnard 1 and NGC 2264C and G are $T_{mb} < 70-100$ mK in 0.11 km s^{-1} channels. For S68N, OMC-2, HH-1 and CB 17, which were observed during daytime, the corresponding upper limits are $T_{mb} < 200-300$ mK.

3.2. Spectra of ND_2H emission

Emission in the $1_{10} \rightarrow 1_{01}$ lines of ND_2H was detected only in Barnard 1; upper limits were obtained in other sources. The spectra have rms levels of $T_{mb} = 5-11$ mK in 0.11 km s^{-1} channels. The ND_2H lines toward Barnard 1 are the strongest observed to date, and the spectra (Fig. 7) are the first ones to show the hyperfine components of the transition. The hyperfine structure has been calculated by L. Coudert (priv. comm.) and the corresponding frequencies and relative strengths are given in Table 4. Our fit to the hyperfine structure, indicates a low optical depth ($\tau < 0.1$) for the lines.

The column densities of ND_2H have been calculated from the observed line strengths, using spectroscopic constants from Roueff et al. (2000). We assume optically thin emission, but take deviations from the Rayleigh-Jeans law into account. Table 5 presents the results. We assume $T_{ex} = 10$ K for positions close to young stellar objects and 5 K for other positions. The numbers given in the table supersede previous values given in van der Tak et al. (2003).

Simultaneous observations of the ND_2H $2_{20}-2_{11}$ line did not result in any detections. Upper limits to T_{mb} range from 11 to 22 mK in 0.11 km s^{-1} channels (T_{sys} of 400−500 K), except for S68N and NGC 1333 (33, −22), where worse weather ($T_{sys} \sim 1000$ K) limited the sensitivity to 40−50 mK.

Table 3. Observed NH_2D line parameters and derived column densities. Numbers in parentheses denote uncertainties in units of the last decimal.

Source	Offset	V_0	ΔV	T_R	τ	T_{ex}	N^a		
	arcsec	km s^{-1}	km s^{-1}	K		K	10^{14} cm^{-2}		
Barnard 1:									
+0	+0	6.78(1)	0.76(2)	1.3(2)	4.0(5)	4(3)	5.8(7)	4.3(5)	2.9(3)
+11	+11	6.76(1)	0.69(4)	2.1(5)	2.5(5)	5(3)	2.1(5)	2.4(5)	1.6(3)
+11	+0	6.82(1)	0.67(2)	2.2(2)	2.7(3)	6(3)	2.2(2)	2.6(2)	1.7(2)
+11	–11	6.88(1)	0.72(3)	1.9(4)	2.6(5)	5(3)	2.6(5)	2.7(5)	1.8(3)
+0	–11	6.80(1)	0.70(3)	1.6(4)	2.7(6)	5(3)	2.9(6)	2.7(5)	1.8(4)
–11	–11	6.66(3)	0.97(6)	1.1(4)	2.5(8)	4(3)	5(2)	3(1)	2.3(8)
–11	+11	6.78(2)	0.74(5)	1.1(3)	3.4(8)	4(3)	5(1)	3.6(9)	2.4(6)
+22	+0	6.83(2)	0.73(6)	2(1)	1.2(7)	6(5)	0.9(5)	1.3(7)	0.9(5)
+22	+11	6.72(2)	0.61(5)	2(1)	1.6(7)	6(4)	1.0(4)	1.4(6)	0.9(4)
+22	–11	6.90(2)	0.70(6)	1.2(5)	2.4(9)	4(3)	3(1)	2.4(9)	1.6(6)
+0	–22	9.21(4)	0.47(7)	0.8(6)	3(2)	4(4)	4(3)	2(1)	1(1)

[a] Values in Col. 8 are for T_{ex} equal to the estimate in Col. 7, and in Cols. 9 and 10 for T_{ex} = 5 K and 10 K, respectively. Uncertainties in N include only those arising from the uncertainties in τ.

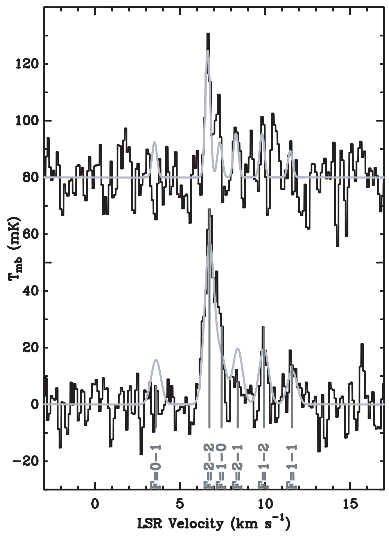

Fig. 7. Spectra of the ND_2H $1_{10}-1_{01}$ ortho (*bottom*) and para (*top*) transitions towards Barnard 1, with our fit to the hyperfine structure overplotted.

Table 4. Frequencies of the hyperfine components of the $1_{10} \rightarrow 1_{01}$ transitions of para and ortho ND_2H.

Transition	ν(MHz)	Relative strength
Ortho		
F = 1–1	110 811.1130	1/12
F = 1–2	110 811.7265	5/36
F = 2–1	110 812.2972	5/36
F = 1–0	110 812.6467	1/9
F = 2–2	110 812.9107	5/12
F = 0–1	110 814.0735	1/9
Para		
F = 1–1	110 895.0298	1/12
F = 1–2	110 895.6433	5/36
F = 2–1	110 896.2108	5/36
F = 1–0	110 896.5635	1/9
F = 2–2	110 896.8243	5/12
F = 0–1	110 897.9823	1/9

3.3. Spectra and maps of ND_3 emission

Table 6 and Fig. 8 summarize the results of the ND_3 observations. In addition, Fig. 9 shows a map of ND_3 in LDN 1689N, with overlaid contours of DCO^+ (3–2) and 1.3 mm dust continuum emission. The emission is seen not to peak on IRAS 16293, ~90″ to the east of the map center, but rather at the outflow interaction region between the YSO and a pre-stellar core. Many deuterated molecules peak at this position, possibly because the outflows from IRAS 16293 A and B, which are not co-eval, have desorbed grain mantles and compressed the gas, which has subsequently cooled (Lis et al. 2002a; Stark et al. 2004). Indeed, the emission peaks at a velocity offset from that of the core (Table 2).

3.4. ND_3 inversion lines

The high-resolution spectrum at the frequency of the strongest hyperfine component of the 1.59 GHz ND_3 inversion line in Barnard 1 is shown in Fig. 10. No emission is detected with a 3σ upper limit for the integrated intensity of 0.011 K km s^{-1},

Table 5. Observed ND_2H line parameters (or 1σ upper limits) and derived column densities. Numbers in parentheses denote uncertainties in units of the last decimal. Positions are the central positions given in Table 2 unless an offset is indicated.

Position	Ortho/	V_0	ΔV	$\int T_{\rm mb} dV$	$T_{\rm ex}$	N(o+p)
	para	km s^{-1}	km s^{-1}	mK km s^{-1}	K	10^{12} cm^{-2}
Barnard 1	o	6.76(2)	0.67(5)	64(4)	5.0	97(6)
	p	6.97(2)	0.34(5)	30(4)	5.0	75(10)
HH-1	o	...	0.5[b]	≤2.7	10.0	≤1.1
	p	...	0.5[b]	≤2.2	10.0	≤1.5
S68N	o	...	0.8[b]	≤2.8	10.0	≤1.1
	p	...	0.8[b]	≤2.8	10.0	≤1.9
NGC 1333:						
(0, 0)	o	...	1.6[a]	≤3.6	10.0	≤1.5
	p	...	1.6[a]	≤3.6	10.0	≤2.5
(0, 11)	o	...	1.6[a]	≤2.2	10.0	≤0.9
	p	...	1.6[a]	≤2.2	10.0	≤1.5
(23, −6)	o	...	1.0[a]	≤2.1	5.0	≤3.2
	p	...	1.0[a]	≤1.8	5.0	≤4.5
(33, −22)	o	...	1.0[a]	≤3.5	5.0	≤5.3
	p	...	1.0[a]	≤3.9	5.0	≤9.7

[a] Value taken from ND_3 (van der Tak et al. 2002).
[b] Value taken from NH_2D (Table 3).

Table 6. Observations of ND_3. Offset positions from nominal central position are given in arc seconds, enclosed in parentheses.

Position	V_0	ΔV	$\int T_{\rm mb} dV$	$T_{\rm ex}$	N
	km s^{-1}	km s^{-1}	K km s^{-1}	K	10^{12} cm^{-2}
NGC 1333	7.2	1.6(6)	0.071(21)	10	0.29(9)[a]
NGC 1333 (23, −6)	6.5	1.0(2)	0.144(43)	5	1.3(4)
NGC 1333 (−24, 106)	7.8	0.7(2)	0.078(17)	5	0.70(15)
Barnard 1 (0, 0)	6.5	0.82(7)	0.307(19)	5	2.8(7)[b]
Barnard 1 (−31, 113)		...	≤0.045	5	≤0.4
LDN 1544C	6.9	0.34(10)	0.120(24)	5	1.1(2)
LDN 1630 (20, 35)	...	...	≤0.096	5	≤0.9
LDN 134N	...	...	≤0.036	5	≤0.32
LDN 1689N (0, 0)	3.3	0.42(4)	0.165(17)	5	1.49(15)
LDN 1689N (−10, −10)	3.4	0.44(3)	0.202(23)	5	1.8(2)
LDN 1689N (0, −20)	3.3	0.42(3)	0.288(26)	5	2.6(2)
LDN 483	5.3	1.5(3)	0.081(19)	5	0.7(2)

[a] van der Tak et al. (2002); [b] Lis et al. (2002). The column density given here is given for $T_{\rm ex} = 5$ K.

computed over a 2 km s^{-1} wide velocity interval and corrected for the main beam efficiency. This upper limit has to be further corrected for the source coupling to the 2.′5 Arecibo beam. The spatial distribution of ND_3 in the Barnard 1 cloud has not been determined. Therefore to estimate the coupling efficiency, we assume that the ND_3 emission has the same spatial distribution as the DCO^+ (3−2) emission, as mapped with the CSO (Lis et al. 2004). The DCO^+ intensity in a 2.5′ beam is decreased by a factor of ∼2 compared to the peak value in the 30″ CSO beam. We thus estimate a 3σ upper limit for the integrated intensity of the 1589.0178 MHz ND_3 inversion line in the CSO beam to be ∼0.022 K km s^{-1}.

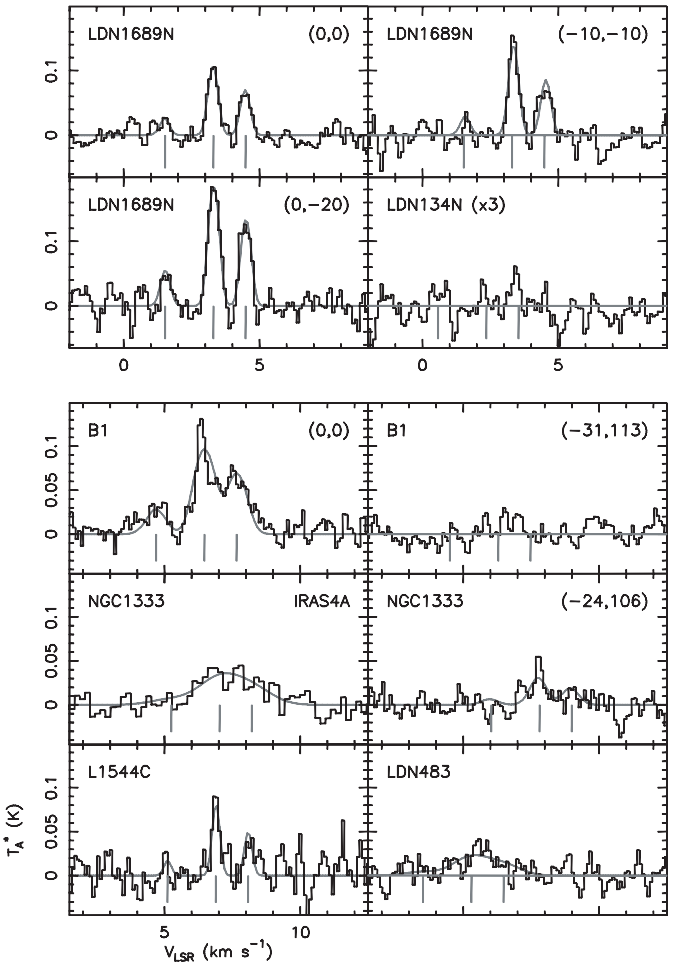

Fig. 8. Spectra of ND_3 309.9 GHz emission, observed with the CSO. The Barnard 1 (B1) spectrum is from Lis et al. (2002) and the NGC 1333 IRAS 4A spectrum from van der Tak et al. (2002).

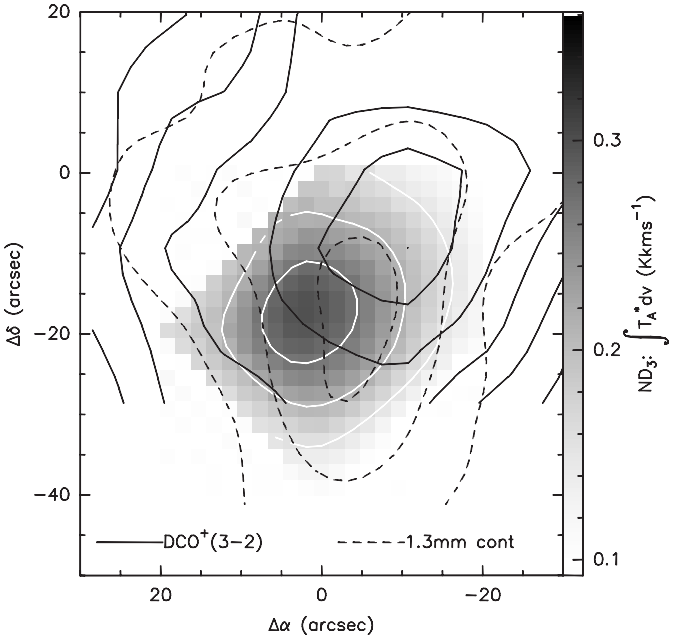

Fig. 9. Intensity of the ND_3 emission in LDN 1689N integrated over velocities between 2.8 and 5 km s^{-1}, (greyscale and white contours), with overlayed contours of $DCO^+(3-2)$ emission (solid black lines) and 1.3 mm dust continuum emission (dashed black lines). The coordinates of the (0, 0) position are RA(J2000) = 16:32:29.5, Dec(J2000) = −24:28:52.6. Contour levels are 50, 70, and 90% of the peak for ND_3, 50 to 90% of the peak, with an interval of 10% for DCO^+, and 4, 6, and 8% of the peak (toward IRAS 16293, outside the plot) for dust continuum.

To compute the corresponding upper limit for the ND_3 column density we use Eq. (2) of Lis et al. (2002b), with $A = 5.23 \times 10^{-11}$ s^{-1}, $g_u = 24$, and $E_u = 11.97$ K, The ND_3 partition function $Q = 38.3$ for $T_{ex} = 10$ K, leading to a 3σ upper limit of 3.0×10^{13} cm^{-2} for the ND_3 column density, after including a factor of 2 correction for the remaining hyperfine components (see Table 7). For $T_{ex} = 5$ K, the partition function $Q = 17.2$ and the corresponding 3σ upper limit for the ND_3 column density is 7.0×10^{13} cm^{-2}. These limits are an improvement over previous Effelsberg results (van der Tak et al. 2003), but still factors of ∼20 above the values derived from the rotational lines (Lis et al. 2002b).

3.5. Summary of ammonia deuterium fractionation

Table 8 lists the column densities and fractionation ratios for ammonia isotopologues in our sample. Only sources where ND_3, or three other isotopologues have been detected are listed. Care was taken that the data are in matching beams (20−40″) whenever possible. For example, there are significant discrepancies in the column density derivations from Shah & Wootten (2001) and Hatchell (2003) towards NGC 1333 IRAS 4A. The NH_3 data for NGC 1333, Barnard 1 and LDN 134N have been taken with the Effelsberg telescope with a ∼40″ beam. Data for LDN 1544C and LDN 483 refer to a larger beam (∼100″) (see references listed in Table 8), and the NH_3 column density for LDN 1544 and LDN 483 may thus be underestimated.

Ammonia fractionation of the various isotopologues is seen to vary from source to source, whereas grain surface chemistry predicts that the deuterium fractionation should scale as atomic D/H ratio, and be constant to within a factor of a few. However, we cannot rule out the grain surface scenario, as the predictions are only qualitative (Rodgers & Charnley 2001). For most sources, $[NH_2D]/[NH_3]$ and $[ND_2H]/[NH_2D]$ ratios are of the same order of magnitude, ∼10−20%, while the $[ND_3]/[ND_2H]$ ratio is significantly smaller (∼2−5%). The assumption of one single excitation temperature for all lines in one source may not be valid, since the lines have very different excitation conditions (Table 1). This uncertainty may affect the column density ratios in Table 8 because the column densities of some isotopologues are derived from ground state lines and others from excited states. From the observational side, the largest uncertainty is thus in the radiative transfer modelling of the data. Collisional cross sections for ammonia isotopologues are needed for a more accurate analysis.

The ND_3 to NH_3 ratio varies between $\sim 1-2 \times 10^{-3}$ in LDN 1689N, Barnard 1, and the depleted core of LDN 1544, where H_2D^+ and D_2H^+ have been detected (Caselli et al. 2003; and Vastel et al. 2004), to less than 1.6×10^{-4} for the dark

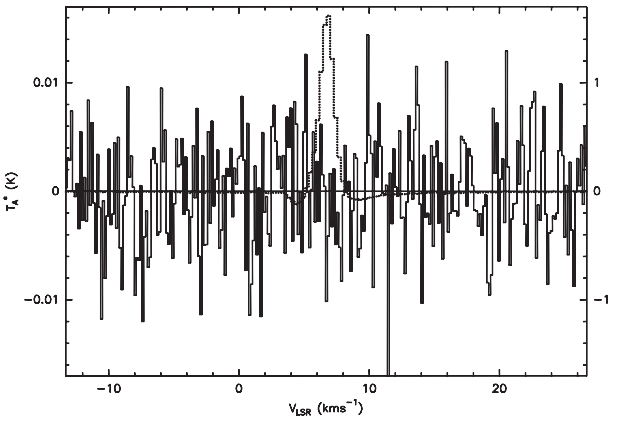

Fig. 10. High-resolution spectrum at the frequency of the 1589.0178 MHz ND_3 hyperfine component in Barnard 1 (left scale). The dotted line shows the 1667.3590 MHz OH line at the same position (right scale).

cloud LDN 134N. Such values represent prodigious enhancement factors over the cosmic ratio of 12 orders of magnitude to less than 11 orders of magnitude which deserve specific chemical studies. We present in the next section a gas phase chemical model and the corresponding detailed results.

4. A model of gas-phase deuterium chemistry

4.1. Approach and general results

We have updated the preliminary gas phase chemical network, which was used to interpret our first detection of ND_3 towards Barnard 1, as presented in Lis et al. (2002b). We have introduced the formation of H_2, HD, and D_2 on grain surfaces by following the simple approach presented in Le Bourlot et al. (1995). The role of the grains (passive, although very significant) is to trap the condensable species, which are then no longer available in the gas phase. The resulting chemical abundances may differ considerably from the so-called typical values, relevant for a standard molecular cloud such as TMC–1. Such effects are labelled as depletion, and observations show a clear correlation of deuterium fractionation and CO depletion in dense pre-stellar cores. This trend results, to first order, from the shorter collision time between dust grains and molecules when the density increases.

In order to mimic this effect, we consider three different models, in which the density and depletion are varied. We consider a "standard" molecular cloud similar to TMC1 with a density of $n(H_2) = 10^4$ cm^{-3}, a temperature T of 10 K and abundances relative to molecular hydrogen of TMC–1, i.e. $[C]/[H_2] = 7\times10^{-5}$; $[O]/[H_2] = 2\times10^{-4}$; $[N]/[H_2] = 2\times10^{-5}$. The relative abundance of sulfur is not well known and is taken as $[S]/[H_2] = 3.6\times10^{-7}$. In addition, we introduce a representative metal [M] which does not contribute to the molecular complexity, and only undergoes charge transfer and radiative recombination reactions, with $[M]/[H_2] = 3\times10^{-8}$ (low metal case). This model is referred as model 1. For all models, we neglect possible deuterium depletion on grains and have adopted a gas phase deuterium abundance of $[D]/[H] = 1.5\times10^{-5}$ as derived from the latest determinations (Linsky 2003). Models 2 and 3 have densities $n(H_2) = 10^5$ cm^{-3} and 10^6 cm^{-3} and carbon and oxygen depletion factors of 5 and 15, respectively. Nitrogen is kept constant in the three models as ISO spectra have not indicated that ammonia ices are abundant. The temperature has been kept equal to 10 K and the cosmic-ray ionization rate is taken as 2×10^{-17} s^{-1}. Table 9 lists the predicted molecular abundances for the three models.

Table 7. ND_3 inversion frequencies within the $J_K = 1_1$ level derived from van Veldhoven et al. (2002).

Transition	ν(MHz)	Relative strength
$F = 0$–1	1587.4645	1/9
$F = 2$–1	1588.3969	5/36
$F = 1$–1	1589.0114	1/12
$F = 2$–2	1589.0086	5/12
$F = 1$–2	1589.6231	5/36
$F = 1$–0	1590.5545	1/9

We consider 210 gas phase species, including H_2, H_2O, CH_4, NH_3, H_2S, H_2CS, all deuterated variants thereof, and corresponding ions. A total of 3000 chemical reactions are included in the chemical network. In addition to the reactions of H_3^+, CH_3^+, $C_2H_2^+$ with HD, which are driving the deuteration as already introduced in Watson (1974), we have considered the subsequent deuteration of molecular hydrogen by introducing the reactions of H_2D^+ and D_2H^+ with HD, D, and D_2 as studied experimentally at low temperatures by Gerlich & Schlemmer (2002). Some of these reactions have also been introduced by Roberts et al. (2004) and by Walmsley et al. (2004) for the completely depleted case. Table 10 gives the fractionation reactions, the rate coefficients of the forward corresponding reaction and the endothermicities involved in the reverse reactions. These values are obtained from the ground level energies without differentiating between ortho and para forms of the various species involved.

As already discussed in Lis et al. (2002b) and Roueff (2005), we have taken special care regarding the dissociative recombination reactions and introduced several updates such as the new dissociative recombination rate coefficient of H_3^+ (McCall et al. 2003), the new branching ratios of the dissociative recombination of N_2H^+ by Geppert et al. (2004), who found that NH is a major product channel and the recent measurement of ND_4^+ (Öjekull et al. 2004). In addition, we have generalized the result of recent studies of dissociative recombination reactions of partially deuterated molecular ions (H_2D^+, HDO^+ and HD_2O^+) which show that the release of H atoms is favoured compared to that of deuterium atoms. We assume that the branching ratios differ by a factor of 2 between H and D ejection, following the recommendations of M. Jensen (private communication)[2]. The influence of this assumption is discussed in Sect. 4.2

[2] In Lis et al. (2002b) we had assumed a factor 3 to 1.

Table 8. Summary of observations of ammonia fractionation.

Source	NH_3	NH_2D	ND_2H	ND_3	$[NH_2D]/[NH_3]$	$[ND_2H]/[NH_2D]$	$[ND_3]/[ND_2H]$	$[ND_3]/[NH_3]$
	10^{15} cm^{-2}	10^{14} cm^{-2}	10^{13} cm^{-2}	10^{12} cm^{-2}				
NGC 1333	1.4 ± 0.4^a	3.9 ± 0.8^a	$\leq 0.5^h$	0.29 ± 0.09^d	0.28 ± 0.14	≤ 0.01	≥ 0.06	$2.1 \pm 1 \times 10^{-4}$
Barnard 1	2.5 ± 0.2^i	5.8 ± 0.7^g	8.6 ± 0.8^h	2.8 ± 0.7^f	0.23 ± 0.05	0.15 ± 0.03	0.033 ± 0.01	$1.1 \pm 0.5 \times 10^{-3}$
LDN 1544C	0.20 ± 0.035^k	0.26 ± 0.01^k		1.1 ± 0.2^e	0.13 ± 0.03			$5.5 \pm 1 \times 10^{-3}$
LDN 134N	2.0 ± 0.2^j	2.0 ± 0.4^b	1.0 ± 0.2^c	$\leq 0.32^e$	0.10 ± 0.03	0.05 ± 0.02	≤ 0.032	$\leq 1.6 \times 10^{-4}$
LDN 1689N	1.8 ± 0.2^k	3.4 ± 0.7^l	7.6 ± 1.1^l	$1.8 \pm 0.2^{e*}$	0.19 ± 0.05	0.22 ± 0.05	0.024 ± 0.01	$1.0 \pm 0.5 \times 10^{-3}$
LDN 483	1.4 ± 0.1^m			0.7 ± 0.2^e				$5.0 \pm 1.2 \times 10^{-4}$

[a] Hatchell (2003); [b] Tiné et al. (2000); [c] Roueff et al. (2000), 20% accuracy assumed; [d] van der Tak et al. (2002); [e] Table 6, * the $-10''$, $-10''$ offset value has been given as it corresponds to the ND_2H peak observed by Loinard et al. (2001), [f] Lis et al. (2002b); [g] Table 3; [h] Table 5; [i] Bachiller et al. (1990), 10% accuracy assumed; [j] Ungerechts et al. (1980), 10% accuracy assumed; [k] Shah & Wootten (2001), 10% accuracy assumed; [l] Loinard et al. (2001); reanalysis of the para transition of NH_2D from the original data; [m] Jijina et al. (1999), Anglada et al. (1997), 10% accuracy assumed.

We can derive the following general trends from these models:

1. The fractional ionization decreases as the density increases, as expected. The main source of electrons is provided by the representative metal which may only recombine or charge transfer and does not contribute to the chemical complexity.
2. The deuterium reservoir is provided by HD. However, as the density increases, molecular D_2 becomes a significant deuterium containing species. It is then important to account properly for the gas phase reactions involving doubly deuterated hydrogen.
3. Model 2 presents the highest molecular fractional abundances for the N-bearing species, while HCN, HNC, and HCO^+ follow the same pattern as C and CO and have higher fractional abundances in model 1.
4. The gas phase chemistry changes significantly between models 2 and 3. Indeed, with the high depletion assumed for model 3, the H_3^+ chemistry is driven by reactions with HD rather than reactions with the abundant neutrals O, CO, etc. This results in significant variations in the fractional abundances of saturated species such as NH_3, HCN, HNC, and HCO^+ and N_2H^+ molecular ions.
5. D_2 is the sole species, which has higher abundance in model 3, as compared to model 2.
6. The combination of high density and depletion results in very efficient production of deuterated species. The abundances of the multiply deuterated species such as D_3^+ and ND_3, are enhanced by between 10 and more than 12 orders of magnitude relative to those expected from the cosmic deuterium abundance, in the various models we have considered.
7. All models predict high fractional abundances of ammonia progenitors such as NH, ND, NH_2, NHD and ND_2.

4.2. Comparison with the observations

We now focus on the comparison of the deuterium fractionation values of the various species with the different observed values. Table 11 reports the deuterium fractionation ratio obtained with the three previously described models and the observed values towards a sample of clouds. We also report the fractionation ratios of nitrogen containing molecules calculated when statistical approximation is assumed for the reaction products coming from dissociative recombination reactions, when the latter have not been studied in the laboratory. The resulting fractionation ratios differ at most by a factor of 2 in the nitrogen containing species.

Following previous remarks, the deuterium fractionation ratio is seen to increase from model 1 to model 3. The D_2H^+/H_2D^+ ratio found in LDN 1689N involves significantly excited levels (the upper level energies of H_2D^+ and D_2H^+ involved are 104 and 83 K, respectively) and may not reflect the actual value of the full D_2H^+/H_2D^+ ratio calculated in our models. Walmsley et al. (2004) and Flower et al. (2004) have considered a completely depleted chemistry with specific para and ortho species and find a p-D_2H^+/o-H_2D^+ consistent with the observations.

However, the ensemble of data for this pre-stellar core (sometimes also called IRAS 16293E) is spectacular. The level of deuteration is particularly high. Stark et al. (2004) deduce a depletion of CO of the order of 5 compared to TMC-1 (from $[C^{18}O]/[H_2] = 3 \times 10^{-8}$ and $[CO]:[C^{18}O] = 500:1$), equal to the value assumed in model 2, and a temperature in the range $12 \leq T \leq 16$ K, whereas we have performed calculations at 10 K. Comparison between model 2 and observations toward LDN 1689N shows an agreement within a factor of 2 for the reported species except for ND_2H which displays a spectacular enrichment. Another source of deuteration than the one assumed may be at work. A plausible mechanism is evaporation from dust grains, resulting from the shocks produced by the outflows, as suggested by Lis et al. (2002a). This hypothesis is also suggested by the detection of doubly deuterated formaldehyde by Ceccarelli et al. (2002) in the same pre-stellar core.

The results displayed for LDN 134N deserve special comments as the search of ND_3 has been very deep and a very low upper limit has been obtained. The density and depletion conditions are probably between those taken for model 2

Table 9. Prediction of fractional abundances relative to molecular hydrogen.

	Model 1	Model 2	Model 3
$n(H_2)$ (cm^{-3})	10^4	10^5	10^6
Depletion	1	5	15
$x(e^-)^a$	6.05×10^{-8}	3.74×10^{-8}	2.91×10^{-8}
H	2.25×10^{-4}	2.26×10^{-5}	2.27×10^{-6}
HD	2.75×10^{-5}	2.65×10^{-5}	2.56×10^{-5}
D	1.22×10^{-6}	4.43×10^{-7}	8.12×10^{-8}
D_2	5.84×10^{-7}	1.49×10^{-6}	2.18×10^{-6}
CO	6.79×10^{-5}	1.33×10^{-5}	4.47×10^{-6}
C	1.72×10^{-6}	5.64×10^{-7}	1.64×10^{-7}
H_3^+	1.03×10^{-8}	3.01×10^{-9}	4.78×10^{-10}
H_2D^+	5.80×10^{-10}	4.45×10^{-10}	1.05×10^{-10}
D_2H^+	3.13×10^{-11}	6.47×10^{-11}	2.33×10^{-11}
D_3^+	1.29×10^{-12}	8.35×10^{-12}	5.20×10^{-12}
NH	4.89×10^{-9}	6.80×10^{-9}	1.66×10^{-9}
ND	1.18×10^{-9}	4.67×10^{-9}	1.70×10^{-9}
NH_2	6.01×10^{-8}	8.48×10^{-8}	1.25×10^{-8}
NHD	2.99×10^{-9}	7.64×10^{-9}	1.51×10^{-9}
ND_2	3.05×10^{-11}	2.05×10^{-10}	5.09×10^{-11}
NH_3	5.49×10^{-8}	8.82×10^{-8}	2.00×10^{-8}
NH_2D	2.71×10^{-9}	8.80×10^{-9}	2.94×10^{-9}
ND_2H	8.82×10^{-11}	6.10×10^{-10}	2.37×10^{-10}
ND_3	3.44×10^{-12}	5.14×10^{-11}	2.14×10^{-11}
HCN	7.13×10^{-8}	3.78×10^{-8}	7.92×10^{-9}
DCN	2.40×10^{-9}	3.15×10^{-9}	8.90×10^{-10}
HNC	3.29×10^{-8}	1.95×10^{-8}	4.02×10^{-9}
DNC	1.54×10^{-9}	2.35×10^{-9}	6.28×10^{-10}
HCO^+	9.67×10^{-9}	1.02×10^{-9}	8.01×10^{-11}
DCO^+	2.85×10^{-10}	6.85×10^{-11}	8.15×10^{-12}
N_2H^+	2.66×10^{-10}	5.28×10^{-10}	1.68×10^{-10}
N_2D^+	9.24×10^{-12}	4.25×10^{-11}	1.80×10^{-11}

[a] Fractional ionization.

(Tiné et al. 2000; Roueff et al. 2000) and model 3 (Pagani et al. 2005). Comparison between models and observed deuterium fractionation ratios is satisfactory except for ND_3 where predictions are above the observed upper limit, and for N_2H^+ which exhibits an impressive deuterium fractionation ratio towards this line of sight. Such values may be obtained within the present treatment if the dissociative recombination rate coefficient of the deuterated N_2D^+ were significantly smaller than that of N_2H^+, a possibility which is not excluded (such effects have been measured for H_3^+ and D_3^+ but not studied experimentally for these nitrogen bearing ions).

The observations in the Barnard 1 molecular cloud are reproduced within a factor of 2 by Model 2 except for ND_2H which is underpredicted by a factor of 3. As temperatures in prestellar clouds can vary between values as low as 7 K in the center and ≃50 K at large radii, we display in Figs. 11 and 12 the relative abundances of deuterated isotopologues of ammonia and of other molecules at temperatures between 5 and 50 K for the conditions pertaining to model 2, with a molecular hydrogen density of 10^5 cm^{-3}. The deuterium fractionation of the various molecules is of the order of 10% for temperatures between 5 and 20 K (except for ND/NH where the value is about unity at low temperatures), and decreases quickly for higher temperatures.

The peak in the deuterium fractionation of ND_3 relative to NH_3 at $T \approx 12$ K is directly linked to the barrier of the reaction of N^+ with HD which is of the order of 16 K (Marquette et al. 1988). Indeed, Jacq et al. (1990) measured lower ammonia fractionation ratio in hot cores ≤0.01 than in the dense cold cores studied here. The temperature dependence

Table 10. Fractionation reactions involving H_3^+, CH_3^+ and $C_2H_2^+$ with HD, D_2 and D.

	k	ΔE	Ref.
	$cm^3\ s^{-1}$	K	
$H_3^+ + HD \rightleftharpoons H_2D^+ + H_2$	3.5(−10)	232	1
$H_2D^+ + HD \rightleftharpoons D_2H^+ + H_2$	2.6(−10)	187	1
$H_3^+ + D_2 \rightleftharpoons H_2D^+ + HD$	1.75(−10)	152	1
$H_3^+ + D_2 \rightleftharpoons D_2H^+ + H_2$	1.75(−10)	340	1
$D_2H^+ + HD \rightleftharpoons D_3^+ + H_2$	2.00(−10)	234	1
$H_2D^+ + D_2 \rightleftharpoons D_2H^+ + HD$	3.50(−10)	109	1
$D_2H^+ + D_2 \rightleftharpoons D_3^+ + HD$	3.50(−10)	100	2
$H_3^+ + D \rightleftharpoons H_2D^+ + H$	1.0(−9)	632	1
$H_2D^+ + D \rightleftharpoons D_2H^+ + H$	1.0(−9)	600	1
$D_2H^+ + D \rightleftharpoons D_3^+ + H$	1.0(−9)	600	4
$CH_3^+ + HD \rightleftharpoons CH_2D^+ + H_2$	2.6(−10)	375	1
$CH_3^+ + D_2 \rightleftharpoons CD_2H^+ + H_2$	4.4(−10)	375	5
$CH_3^+ + D_2 \rightleftharpoons CH_2D^+ + HD$	6.6(−10)	375	1
$CH_2D^+ + HD \rightleftharpoons CD_2H^+ + H_2$	1.0(−9)	370	1
$CH_2D^+ + D_2 \rightleftharpoons CD_3^+ + H_2$	3.0(−10)	370	3
$CH_2D^+ + D_2 \rightleftharpoons CD_2H^+ + HD$	9.0(−10)	370	3
$CD_2H^+ + HD \rightleftharpoons CD_3^+ + H_2$	5.64(−10)	370	3
$CD_2H^+ + D_2 \rightleftharpoons CD_3^+ + HD$	4.5(−10)	370	3
$C_2H_2^+ + HD \rightleftharpoons C_2HD^+ + H_2$	7.5(−10)	550	1
$C_2HD^+ + HD \rightleftharpoons C_2D_2^+ + H_2$	7.5(−10)	300	1
$C_2H_2^+ + D_2 \rightleftharpoons C_2HD^+ + HD$	7.0(−10)	550	2
$C_2HD^+ + D_2 \rightleftharpoons C_2D_2^+ + HD$	7.0(−10)	550	2
$C_2H_2^+ + D \rightleftharpoons C_2HD^+ + H$	7.5(−10)	250	2
$C_2HD^+ + D \rightleftharpoons C_2D_2^+ + H$	7.5(−10)	150	2

References: 1. Gerlich et al. (2002); 2. estimate; 3. Smith et al. (1982); 4. Walmsley et al. (2004); 5. Anicich (2003).

is discussed by Shah & Wootten (2001). The ammonia fractionation remains close to 10% for a kinetic temperature below 30 K, but drops to a few percent in warmer regions. The turnover in the model presented here occurs at a slightly lower temperature (22 K), but the overall shape is fairly well reproduced, given the uncertainty in the observed temperature measurements.

Another interesting feature is seen in Fig. 12, where the modelled DCN/HCN ratio is found to be smaller than that of DNC/HNC at temperatures below 20 K, whereas the opposite is found at higher temperatures. This trend is clearly found towards LDN 134N which is known to be a cold source. Such a tendency had already been emphasized by Roueff & Gerin (2003) for a sample of dark cold sources. We have been led to carefully consider the various channels leading to deuterated HCN and HNC which are produced, in such gas phase chemistry, via the dissociative recombination of $HCND^+$, $DCNH^+$ and $HDNC^+$. Table 12 displays the values assumed.

We note that this prediction is not derived in the accretion models of Roberts et al. (2004). DCN/HCN and DNC/HNC ratios become closer in LDN 1689N where the temperature may be around 16 K as discussed by Mizuno et al. (1990) and Stark et al. (2004), in nice agreement with the model predictions. In addition, we display the temperature dependence of the deuterium fractionation ratios of the HCO^+ and N_2H^+ molecular ions, which are very similar.

The ND_3 to NH_3 ratio is highest for LDN 1544. However, the ammonia column density in this source may be underestimated because of the large beam size of the observations. High fractionations are also obtained for Barnard 1 and LDN 1689N, for which we could benefit from higher quality ammonia data. We therefore believe that the correction for the ammonia column density is at most a factor of three and the ND_3 to NH_3 ratio in LDN 1544 is close to the values obtained in Barnard 1 and LDN 1689N. This line of sight is well studied and known to be a highly depleted core (Caselli et al. 2003). The observations and the results of model 3 agree within a factor of 3. Roberts et al. (2004) have made detailed modelling of LDN 1544 by introducing the density and temperature structure of this prestellar core in a model including accretion processes on dust grains and an extensive chemical network. The overall predicted deuterium fractionation is larger by about one order of magnitude than the present observations. However, a nice agreement between models and observations is obtained for doubly deuterated formaldehyde by Roberts et al. (2004).

Extremely young protostars have been found in the Barnard 1 molecular cloud (Hirano et al. 1999) and the depletion factor is about 3 compared to TMC-1 (cf. Lis et al. 2002b). Recent observations have revealed the presence of HDS, D_2S (Vastel et al. 2003), HDCS and D_2CS (Marcelino et al. 2005) in this dark cloud, which deserves a specific chemical analysis. The level of deuteration is quite high and probably involves a source of deuteration in addition to that provided by gas phase chemistry alone.

5. Conclusions

The present study reports detection of fully deuterated ammonia towards 5 lines of sight, with derived ND_3/NH_3 ratios between 2×10^{-4} and $1{-}2 \times 10^{-3}$ in various pre-stellar cores. A very low upper limit for this ratio (1.6×10^{-4}) has been found towards the dense dark cloud LDN 134N. These observations imply a tremendous enhancement factor over the cosmic deuterium/hydrogen value which varies from about 11 to over 12 orders of magnitude. The spatial extension is limited and the ND_3 peak does not coincide with the DCO^+ peak in LDN 1689N, a source where such a study is possible thanks to its exceptionally high deuterium enhancement. Deuterated species do not peak towards protostars themselves, but at offset positions, suggesting that protostellar activity decreases deuteration built in the pre-stellar phase. We have studied the origin of the deuterium enrichment in terms of a steady state gas phase chemical model, which includes a limited number of molecules, but which allows full deuteration of basic important intermediates. The role of grains is simulated by introducing different values of the depletion of C and O so that the

Table 11. Comparison between predicted and observed deuterium fractionation.

	Model 1	Model 2	Model 3	LDN 134N	LDN 1689N	Barnard 1	LDN 1544
D:H	0.0054	0.020	0.031				
D_2:HD	0.022	0.056	0.083				
H_2D^+:H_3^+	0.056	0.15	0.22				
D_2H^+:H_2D^+	0.054	0.14	0.22		0.75[a]		
D_3^+:D_2H^+	0.043	0.15	0.27				
D_3^+:H_3^+	1.32×10^{-4}	3.15×10^{-4}	0.013				
NH_2D:NH_3	0.049	0.10	0.15	0.1[b]	0.19[b]	0.23[b]	0.13[b]
NH_2D:NH_3*	0.025	0.052	0.077				
ND_2H:NH_2D	0.032	0.069	0.080	0.05[b]	0.22[b]	0.15[b]	
ND_2H:NH_2D*	0.021	0.040	0.049				
ND_3:ND_2H	0.039	0.084	0.090	≤0.032	0.024[b]	0.033[b]	
ND_3:ND_2H*	0.035	0.075	0.078				
ND_3:NH_3	6.3×10^{-5}	5.8×10^{-4}	1.1×10^{-3}	$\leq 1.6 \times 10^{-4}$	1.0×10^{-3}[b]	1.1×10^{-3}[b]	5.4×10^{-3}[b]
DCN:HCN	0.034	0.083	0.11	0.06[c]	0.11[e]		
DCN:HCN*	0.019	0.049	0.075				
DNC:HNC	0.047	0.12	0.16	0.12[f]	0.091[f]		0.050[g]
DNC:HNC*	0.029	0.071	0.091				
DCO^+:HCO^+	0.030	0.067	0.10	0.18[d]	0.08[e]		0.04[h]
N_2D^+:N_2H^+	0.035	0.087	0.11	0.35[d]		0.15[i]	0.2[h]

* Models employing a statistical approximation for the reaction products in dissociative recombination reactions of non studied deuterated molecular ions.

[a] Vastel et al. (2004), para-D_2H^+/ortho-H_2D^+; [b] Table 8; [c] Turner (2001), based on $N(HN^{13}C) \times 60$; [d] Tiné et al. (2000); [e] Lis et al. (2002a), based on $N(H^{13}CN)$ and $N(H^{13}CO^+) \times 60$; [f] Hirota et al. (2001), based on $N(HN^{13}C) \times 60$; [g] Hirota et al. (2003), based on $N(HN^{13}C) \times 60$; [h] Caselli et al. (2002); [i] Gerin et al. (2001).

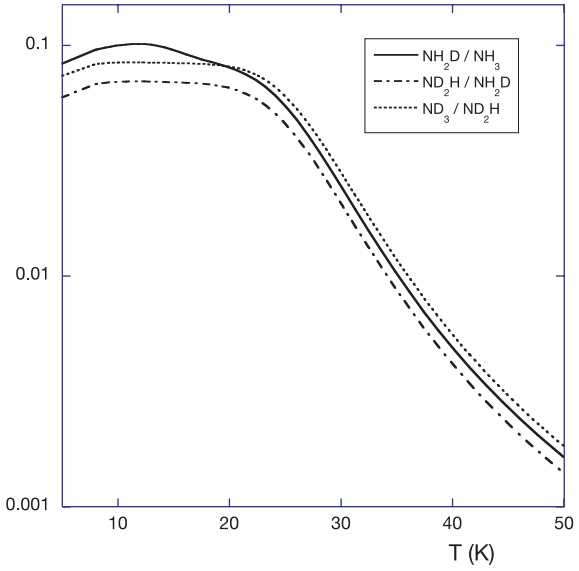

Fig. 11. Results of model calculations of the ratio of different deuterated isotopologues of ammonia as a function of temperature. The conditions of model 2 have been employed. The full line shows NH_2D relative to NH_3 the dotted line shows ND_2H relative to NH_2D and the dash-dotted line shows ND_3 reltive to ND_2H. Note that ND_2H relative to NH_2D is the lowest ratio for all the temperatures considered in this calculation.

important deuterated molecular ions H_2D^+, D_2H^+, D_3^+, CH_2D^+, CD_2H^+, CD_3^+ are not destroyed by reactions with O, CO, ... in the highly depleted regions. Our models make the following predictions:

- Higher density models with higher C and O depletions yield greater enhancement of the relative abundances of the deuterated ammonia isotopologues.
- The models predict abundance ratios of the deuterated ammonia isotopologues, which agree reasonably well with new and existing observations.
- The fractionation ratios of ammonia deuterated isotopologues remain large for temperatures as high as 20 K.
- The temperature dependence of the ratios DCN/HCN and DNC/HNC is not identical. Whereas DNC/HNC is larger at low temperatures, the opposite becomes true at higher temperatures.
- A very high deuterium fractionation is predicted for ND. We also find a significant abundance of NHD in our models. Both species have rotational transitions in the submillimeter domain and are potentially detectable from the ground.
- D_2 may be an important component of the cloud and the corresponding reactions have to be introduced. There is, unfortunately, no hope of detecting it under the conditions which characterize cold, dark clouds.

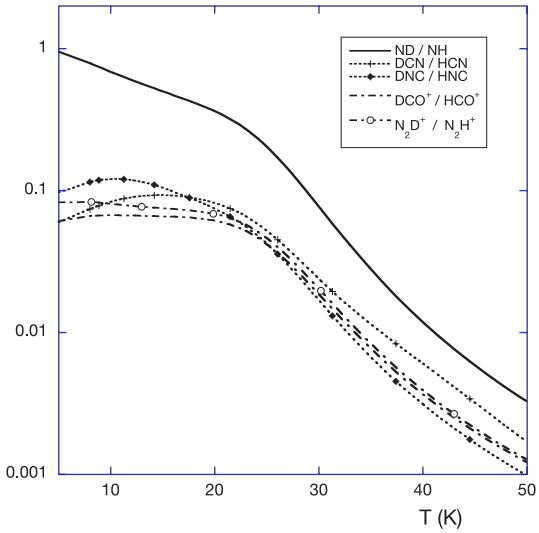

Fig. 12. Results of model calculations of the ratio of different deuterated isotopologues of nitrogen containing molecules as a function of temperature. The conditions of model 2 have been employed. The full line displays ND/NH, crosses and diamonds on the dotted line shows DCN/HCN and DNC/HNC respectively whereas the dashed-dotted line without and with open circles refer to DCO^+/HCO^+ and N_2D^+ and N_2H^+ respectively.

Table 12. Assumed reaction rate coefficients and branching ratios in dissociative recombination reactions of deuterated $HCNH^+$ and H_2NC^+.

Reaction			k (in 10^{-7} cm^3 s^{-1})
$HCND^+$ + electron	→	HCN + D	1.16 $(T/300)^{-0.5}$
		DNC + H	2.33 $(T/300)^{-0.5}$
$DCNH^+$ + electron	→	DCN + H	2.33 $(T/300)^{-0.5}$
		HNC + D	1.16 $(T/300)^{-0.5}$
$HDNC^+$ + electron	→	HNC + D	0.58 $(T/300)^{-0.5}$
		DNC + H	1.16 $(T/300)^{-0.5}$
		NHD + C	1.75 $(T/300)^{-0.5}$

Acknowledgements. The authors thank the staffs of the Arecibo, CSO and IRAM 30 m telescopes for their support. IRAM is an international institute for research in millimeter-wave astronomy, co-funded by the Centre National de la Recherche Scientifique (France), the Max Planck Gesellschaft (Germany) and the Instituto Geografico Nacional (Spain). The CSO is funded by the US. NSF through contract AST 22-09008. The Arecibo Observatory is part of the National Astronomy and Ionosphere Center, which is operated by Cornell University under a cooperative agreement with the National Science Foundation. We thank Laurent Coudert who calculated for us the hyperfine structure of the various deuterated isotopologues of ammonia. M.G. and E.R. acknowledge travel support from the CNRS/INSU research program PCMI.

References

Anglada, G., Sepulveda, I., & Gomez, J. F. 1997, A&AS, 121, 255
Anicich, V. 2003, An Index of the Literature for Bimolecular Gas Phase Cation-Molecule Reaction Kinetics, Publication 03-19, JPL
Bachiller, R., del Rio Alvarez, S., & Menten, K. M. 1990, A&A, 236, 461
Bacmann, A., Lefloch, B., Ceccarelli, C., et al. 2002, A&A, 389, L6
Bacmann, A., Lefloch, B., Ceccarelli, C., et al. 2003, ApJ, 585, L55
Caselli, P., van der Tak, F. F. S., Ceccarelli, C., & Bacmann, A. 2003, A&A, 403, L37
Caselli, P., Walmsley, C. M., Zucconi, A., et al. 2002, ApJ, 565, 344
Ceccarelli, C., Castets, A., Loinard, L., Caux, E., & Tielens, A. G. G. M. 1998, A&A, 338, L43
Ceccarelli, C., Vastel, C., Tielens, A. G. G. M., et al. 2002, A&A, 381, L17
Dartois, E., Schutte, W., Geballe, T. R., et al. 1999, A&A, 342, L32
Dartois, E., Thi, W.-F., Geballe, T. R., et al. 2003, A&A, 399, 1009
Flower, D. R., Pineau des Forêts, G., & Walmsley, C. M. 2004, A&A, 427, 887
Geppert, W. D., Thomas, R., Semaniak, J., et al. 2004, ApJ, 609, 459
Gerin, M., Pearson, J. C., Roueff, E., Falgarone, E., & Phillips, T. G. 2001, ApJ, 551, L193
Gerlich, D., Herbst, E., & Roueff, E. 2002, Planet. Space Sci., 50, 1275
Gerlich, D., & Schlemmer, S. 2002, Planet. Space Sci., 50, 1287
Gibb, E. L., Whittet, D. C. B., Schutte, W. A., et al. 2000, ApJ, 536, 347
Hatchell, J. 2003, A&A, 403, L25
Hirano, N., Kamazaki, T., Mikami, H., Ohashi, N., & Umemoto, T. 1999, in Star Formation 1999, ed. T. Nakamoto, Nobeyama Radio Observatory, 181
Hirota, T., Ikeda, M., & Yamamoto, S. 2001, ApJ, 547, 814
Hirota, T., Ikeda, M., & Yamamoto, S. 2003, ApJ, 594, 859
Jacq, T., Walmsley, C. M., Henkel, C., et al. 1990, A&A, 228, 447
Jijina, J., Myers, P. C., & Adams, F. C. 1999, ApJS, 125, 161
Le Bourlot, J., Pineau des Forets, G., Roueff, E., & Flower, D. R. 1995, A&A, 302, 870
Linsky, J. L. 2003, Space Sci. Rev., 106, 49
Lis, D. C., Gerin, M., Phillips, T. G., & Motte, F. 2002a, ApJ, 569, 322
Lis, D. C., Gerin, M., Roueff, E., & Phillips, T. G. 2004, in The Dense Interstellar Medium in Galaxies, 487
Lis, D. C., Roueff, E., Gerin, M., et al. 2002b, ApJ, 571, L55
Loinard, L., Castets, A., Ceccarelli, C., Caux, E., & Tielens, A. G. G. M. 2001, ApJ, 552, L163
Marcelino, N., Cernicharo, J., Roueff, E., Gerin, M., & Mauersberger, R. 2005, ApJ, 620, 308
Marquette, J. B., Rebrion, C., & Rowe, B. R. 1988, J. Chem. Phys., 89, 2041
McCall, B. J., Huneycutt, A. J., Saykally, R. J., et al. 2003, Nature, 422, 500
McMullin, J. P., Mundy, L. G., Blake, G. A., et al. 2000, ApJ, 536, 845
Mizuno, A., Fukui, Y., Iwata, T., Nozawa, S., & Takano, T. 1990, ApJ, 356, 184
Öjekull, J., Andersson, P. U., Någård, M. B., et al. 2004, J. Chem. Phys., 120, 7391
Pagani, L., Pardo, J.-R., Apponi, A. J., Bacmann, A., & Cabrit, S. 2005, A&A, 429, 181
Parise, B., Castets, A., Herbst, E., et al. 2004, A&A, 416, 159
Parise, B., Ceccarelli, C., Tielens, A. G. G. M., et al. 2002, A&A, 393, L49
Parise, B., Simon, T., Caux, E., et al. 2003, A&A, 410, 897
Pontoppidan, K. M., Dartois, E., van Dishoeck, E. F., Thi, W.-F., & d'Hendecourt, L. 2003, A&A, 404, L17
Roberts, H., Herbst, E., & Millar, T. J. 2003, ApJ, 591, L41
Roberts, H., Herbst, E., & Millar, T. J. 2004, A&A, 424, 905
Roberts, H., & Millar, T. J. 2000, A&A, 361, 388

Rodgers, S. D., & Charnley, S. B. 2001, ApJ, 553, 613
Roueff, E. 2005, J. Phys.: Conf. Ser., 4, 1
Roueff, E., & Gerin, M. 2003, Space Sci. Rev., 106, 61
Roueff, E., Tiné, S., Coudert, L. H., et al. 2000, A&A, 354, L63
Shah, R. Y., & Wootten, A. 2001, ApJ, 554, 933
Smith, D., Adams, N. G., & Alge, E. 1982, ApJ, 263, 123
Stark, R., Sandell, G., Beck, S., et al. 2004, ApJ, 608, 341
Stark, R., van der Tak, F. F. S., & van Dishoeck, E. F. 1999, ApJ, 521, L67
Tielens, A. G. G. M. 1983, A&A, 119, 177
Tiné, S., Roueff, E., Falgarone, E., Gerin, M., & Pineau des Forêts, G. 2000, A&A, 356, 1039
Turner, B. E. 1990, ApJ, 362, L29
Turner, B. E. 2001, ApJS, 136, 579
Ungerechts, H., Walmsley, C. M., & Winnewisser, G. 1980, A&A, 88, 259
van der Tak, F. F. S., Lis, D. C., Gerin, M., et al. 2003, in Chemistry as a diagnostic of star formation, 50
van der Tak, F. F. S., Schilke, P., Müller, H. S. P., et al. 2002, A&A, 388, L53
van Veldhoven, J., Jongma, R. T., Sartakov, B., Bongers, W. A., & Meijer, G. 2002, Phys. Rev. A, 66, 032501
Vastel, C., Phillips, T. G., Ceccarelli, C., & Pearson, J. 2003, ApJ, 593, L97
Vastel, C., Phillips, T. G., & Yoshida, H. 2004, ApJ, 606, L127
Walmsley, C. M., Flower, D. R., & Pineau des Forêts, G. 2004, A&A, 418, 1035
Watson, W. D. 1974, ApJ, 188, 35